Understanding the role of aluminum-based activators in single site iron catalysts for ethylene oligomerization.

Zoubeyr Boudene, Adrien Boudier, Pierre-Alain Breuil, Hélène Olivier-Bourbigou, Pascal Raybaud, Hervé Toulhoat, Theodorus de Bruin

Understanding the Role of Aluminum-Based Activators in Single Site Iron Catalysts for Ethylene Oligomerization

Zoubeyr Boudene,[1] Adrien Boudier,[2] Pierre-Alain R. Breuil,[2] Hélène Olivier-Bourbigou,[2] Pascal Raybaud,[2] Hervé Toulhoat[1] and Theodorus de Bruin*,[1]

IFP Energies nouvelles, 1 & 4 avenue de Bois-Préau, 92852 Rueil-Malmaison, France.

IFP Energies nouvelles, Rond-point de l'échangeur de Solaize, BP3, 69360 Solaize, France

Corresponding Author:

Theodorus de Bruin

IFP Energies Nouvelles

1 & 4 Avenue de Bois-Préau

92852 Rueil-Malmaison

France

Tel. +33 1 47 52 54 38

Email : theodorus.de-bruin@ifpen.fr

ABSTRACT: In a combined experimental and theoretical study the activation process of a single site ethylene oligomerization catalyst with aluminum based activators has been studied. The results put forward a plausible deactivation reaction path of the catalyst for trimethylaluminum, while for methylaluminoxane and a novel phenoxyaluminum-based activator the experimental catalyst's activity correlates with the energy barrier for the ethylene insertion.

Graphical Abstract

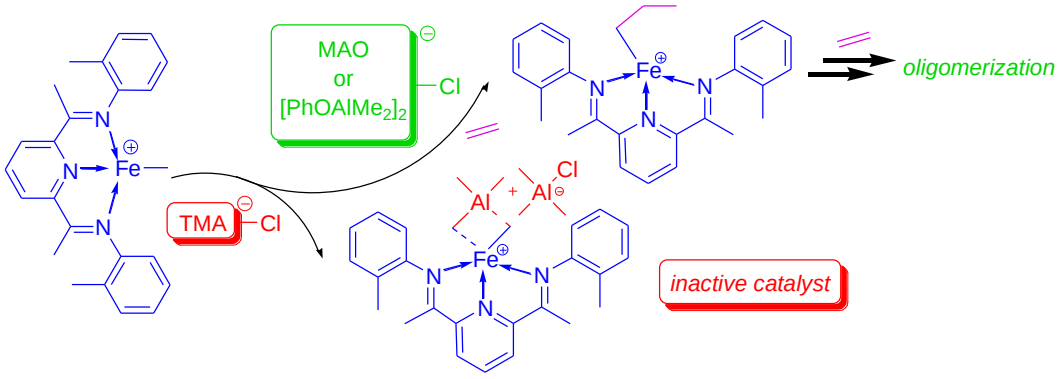

Keywords: Homogeneous catalysis; oligomerization; ethylene; catalyst activation; cocatalyst; methylaluminoxane; mechanism; DFT; molecular modeling.

1. Introduction

Methylaluminoxanes (MAO) [1–4] have been widely used as activators of ethylene oligomerization and polymerization iron-based catalysts, especially those belonging to the bis(imino)pyridine family, affording highly productive catalytic systems [5–12]. As high MAO/metal ratios are required, leading to high costs, considerable efforts have been undertaken to replace them in oligomerization reactions [13–15]. This requires a good understanding of the activation process of the catalyst. However, the identification of the precise role and active center of MAO during the activation process is hampered by the multitude of aluminum species present in solution [16,17], the control of the reaction exothermicity, along with the catalyst degradation and polymer byproduct formation.

In this communication we report a well-defined dimeric aluminum complex $[PhOAlMe_2]_2$ and its activity for ethylene oligomerization using ($\{2,6\text{-}(2\text{-}(CH_3)C_6H_4N{=}C(CH_3))_2\text{-}C_5H_3N\}Fe(II)Cl_2$) (abbreviated as $LFeCl_2$) precursor in comparison with the MAO and trimethylaluminium (TMA) cocatalysts. We furthermore present the DFT simulations that helping to explain the observed

experimental activities. $[PhOAlMe_2]_2$ and TMA are structurally well-defined aluminum species, whereas MAO is not. For the latter, a previously described model is therefore used (Scheme 1, structure (iii) in the lower rectangular box) [18–20].

While the iron-catalyzed oligomerization mechanism is largely accepted to follow a Cossee-Arlman type mechanism, leading to a Schulz-Flory distribution of linear α-olefins, the debate concerning the nature of the metallic active species and the corresponding activation path remains open and is fuelled with numerous studies regarding the oxidation state of the active species or the non-innocence of the ligand towards redox reactions [21–26]. For example, $[LFe(II)Me]^+$ was observed by mass spectrometry along with other cationic species after activation of $[LFe(II)Cl_2]$ by MAO. We here assume a high-spin ferrous iron cationic species after activation with a redox-innocent neutral bis(imino)pyridine chelate and suppose no electron transfers between the metal and ligand.

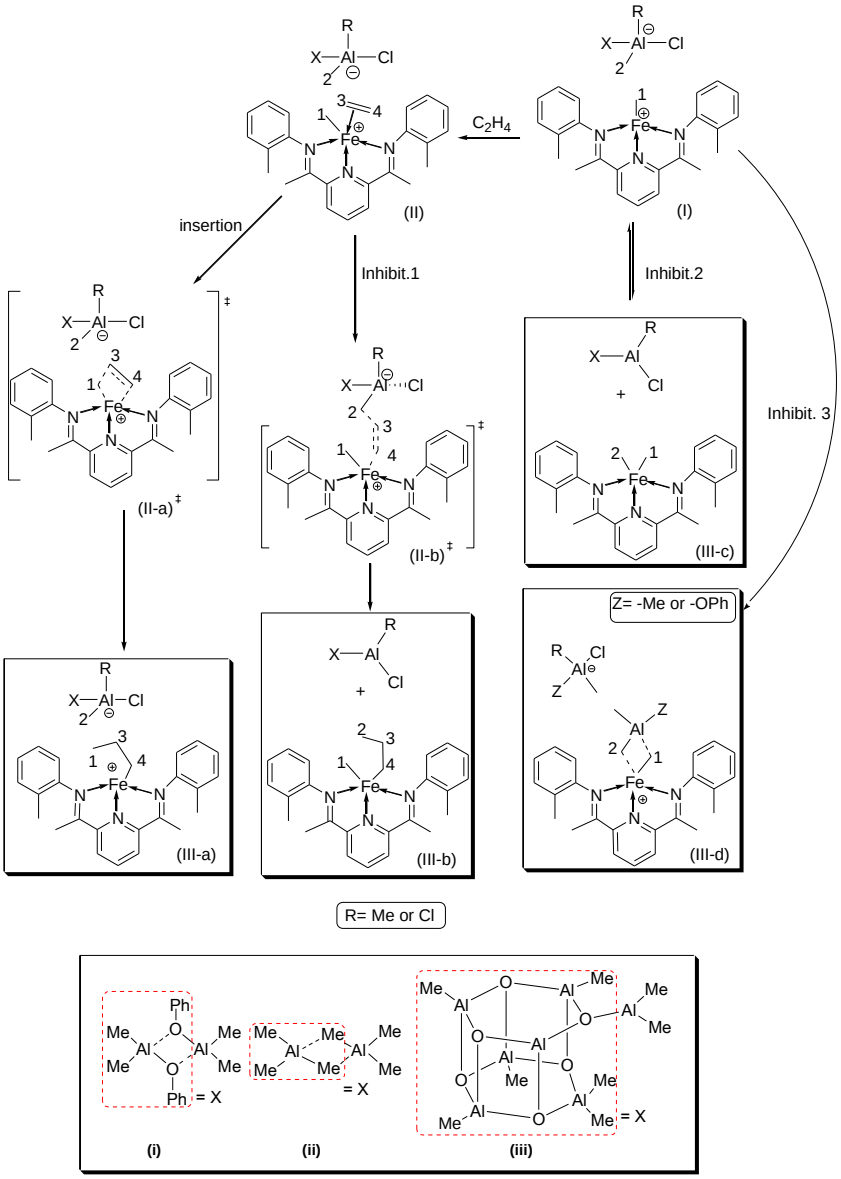

Scheme 1. Pathways for ethylene insertion and catalyst inhibition.

2. Materials and Methods

Methylaluminoxane (MAO 10 wt % in toluene) and TMA (trimethylaluminum) were purchased from Chemtura, while $[PhOAlMe_2]_2$ was obtained by addition of an equimolar amount of phenol to TMA in *n*-heptane in good yield (97 %) and was characterized by ^{1}H and ^{13}C NMR and XRD [27]. $[LFe(II)Cl_2]$ was prepared according to the procedure described in ref [28].

A toluene solution containing [LFe(II)Cl_2] (10 μmol) was injected in the autoclave under an inert nitrogen atmosphere, followed by the cocatalyst solution. The ethylene pressure was immediately increased to 30 bar, the temperature to 50 °C and the mixture was mechanically stirred. Additional details are provided in the Supplementary Materials.

DFT calculations were carried out with the unrestricted M06 functional [29], proven to provide an accurate description of aluminoxanes [30] as well as the spin state of the iron catalyst (Table 5S), in combination with Los Alamos pseudopotential and associated valence basis set on iron atoms [31] and the basis set 6-31G(d,p) for the other atoms. We have verified that inclusion of solvent effects or expansion of the wave-functions over larger basis sets do not change the conclusions presented below from results of gas phase DFT calculations. This is in line with the theoretical findings of Zurek and Ziegler who also concluded that relative energies were not impacted by the inclusion of a solvent model [19]. Further details are presented in the supplementary materials.

3. Results and discussion

Zero oligomerization activity was observed with the [LFe(II)Cl_2]/TMA system, even with an Al/Fe molar ratio of 500, while at the same ratio an activity up to 1.4×10^5 g·(mol(Fe)·h)$^{-1}$ was measured with [PhOAlMe_2]$_2$. Ideally, lower Al to Fe ratios are sought after, as put forward in the introduction, but this leads to lower oligomerization activities.

A Schulz-Flory distribution (K = 0.68) of linear α-olefins was afforded comparable to the one observed when the activation is performed with MAO (Al/Fe = 250, K = 0.69). This latter catalytic system showed a higher, up to 7.4×10^7 g·(mol(Fe)·h)$^{-1}$, activity. Nevertheless, the iron bis(imino)pyridine/MAO system is temperature-sensitive and coupled to the important

exothermicity of the reaction, processing issues are encountered even at low catalyst loading. In our case, more than 40 wt% of the formed products are waxes and polyethylene (PE) with this system, while none of these heavy products were obtained with $[PhOAlMe_2]_2$.

As $[PhOAlMe_2]_2$ is a structurally well-defined cocatalyst, it serves as a very good candidate in this theoretical study to help to elucidate the activation mechanism of the precatalyst using MAO.

$[LFe(II)Me]^+$ may be obtained from $[LFe(II)Cl_2]$ after a transfer of the two chloride anions to the cocatalyst, which becomes either mono- or dichlorinated, while Fe(II) gets mono-methylated. These initial steps have been studied with DFT calculations for the TMA and $[PhOAlMe_2]_2$ cocatalyts. Only minor energy differences between the reaction intermediates were found for both systems, thus not explaining the experimental activity difference. Since moreover, the complete dissociation of the created cationic iron species and the anionic cocatalyst is prohibitively costly, we will focus on the reactions of the ion pair, i.e., cationic monoalkyl $[LFe(II)Me]^+$ and investigate its interactions with the three cocatalysts, each being mono- or dichlorinated (Figure 5S) as well as with ethylene.

Table 1 shows that only the formation of the monochlorinated TMA anion is an exergonic reaction. For $[PhOAlMe_2]_2$ and the MAO model chloride anion formation is endergonic and moreover the dichloride anion is thermodynamically slightly more stable. Since the energy difference is small between the mono- and dichlorinated anion both intermediates will be

considered in this study. This endergonicity puts forward an additional reason[1] why such large excesses of $[PhOAlMe_2]_2$ and MAO are needed to activate.

Table 1. Calculated Gibbs energies ($kcal \cdot mol^{-1}$) to form the mono- and dichlorinated anionic cocatalyst.

	$[PhOAlMe_2]_2$	TMA dimer	$[AlMeO]_6[AlMe_3]$
Monochlorinated	13.2	–0.6	5.9
Dichlorinated	11.6	6.5	2.4

In the following we assume that each cocatalyst is able to generate the $[LFe(II)Me]^+$ species; we first show how the nature of the anion influences the ethylene insertion mechanism: (**II**) → (**III-a**) in Scheme 1. In parallel, we explore possible routes leading to the catalyst deactivation: (**II**) → (**III-b**), (**II**) → (**III-c**) and (**II**) → (**III-d**).

The ethylene uptake by (**I**) yields intermediate (**II)**, where the coordinated ethylene can be inserted in the Fe-C[1] bond to give (**III-a**). The intermediates and transition states (**II-a**‡) for the insertion of ethylene into the Fe-C bond were optimized in the presence of the different chlorinated anionic activators (Figure 6S). For each ion-pair, an equatorial and axial approach (Figure 4S) of the ethylene molecule has been evaluated and only the most stable π-complex was

[1] Other evoked reasons are the partial "loss" of MAO due to reactions with impurities (scavenger effect, ref. [4]) and minor presence of reactive aluminum sites in MAO oligomers, as shown in ref [30].

retained. The calculated Gibbs energies for different optimized intermediates and transition states are reported in Figure 1.

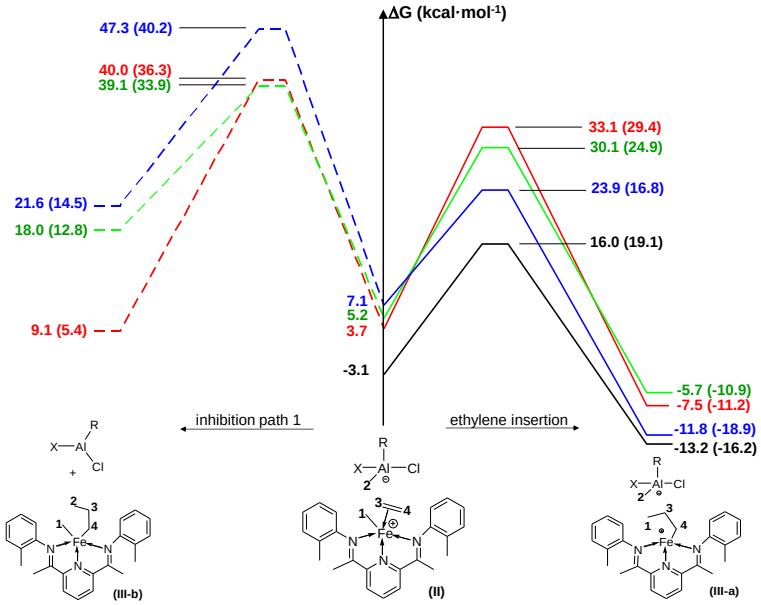

Figure 1. Gibbs energy profiles (kcal·mol^{-1}) for the ethylene insertion step (right) and inhibition path 1 (left) for $[PhOAlMe_2]_2$ (green), TMA (red), $[AlMeO]_6[AlMe_3]$ (blue) and bare catalyst (black). Energies are relative to the energy of the ion-pair and the ethylene molecule at infinite distance (values between parentheses are relative to the energies of the π-complexes).

The ethylene uptake is endergonic for all ion pairs obtained from the activation with the three different mono- or dichlorinated anions, note that the reported energies are relative to the energies of the ion pair and ethylene molecule at infinite distance. Considering the monochlorinated counter ions, the Gibbs energy barriers for the ethylene insertion are 16.8, 24.9 and 29.4 kcal·mol^{-1} for respectively $[AlMeO]_6[AlMe_3]$, $[PhOAlMe_2]_2$ and TMA. Interestingly, the energy barrier for the insertion with the MAO model is even slightly lower than the value obtained for

the bare cationic π-complex ($\Delta G^{\ddagger}$ = +19.1 kcal·mol^{-1}). However, the relative energy is lower for the bare complex.

The energy barrier for ethylene insertion is influenced by different parameters, like the interaction of the π-complex with the counterion. Hence, the smaller dissociation energy of the anion, i.e. 60.7, 67.8 and 81.0 kcal·mol^{-1} for respectively, MAO, $[PhOAlMe_2]_2$ and TMA, the lower the barrier. Also the change in the C–C ethylene distance in going from the π-adduct to the transition state, convincingly correlates with the energy barrier: the smallest changes are observed for the smallest barrier energies, where the ethylene is weakly coordinated, e.g. in the bare complex and in presence of the MAO (see Table 3S and Figure 2S).

The effect of the presence of dichlorinated anions on the uptake of ethylene and the insertion path has also been calculated. Especially, the formation of the π-adduct in presence of the dichlorinated phenoxy species, $[Al_2Ph_2O_2Me_3Cl_2]^-$, becomes disfavored: ΔG_r = +13.7 kcal·mol^{-1} (Figure 1S) with respect to the monochlorinated form (ΔG_r = +13.7 kcal·mol^{-1}). With a barrier of 20.7 kcal·mol^{-1} for the ethylene insertion, the TS consequently gets as well significantly destabilized, making the overall insertion step slightly endergonic (ΔG_r = +2.0 kcal·mol^{-1}). Since $[PhOAlMe_2]_2$ experimentally does activate $[LFe(II)Cl_2]$, we conclude that the monochlorinated anion is involved in the activation process, as it exhibits the more favorable (kinetic and thermodynamic) pathway. The dichlorinated form of TMA and MAO influences considerably less the stability of the π-complex and the insertion barrier, as can be seen from Figure 1S.

The free energy barrier for ethylene insertion is lower in case of $[AlMeO]_6[AlMe_3]$ than for $[PhOAlMe_2]_2$ or TMA, thereby providing an explanation for the higher experimental oligomerization activities. However, the calculated activation energy barriers do not explain the

experimental zero activity with TMA. Therefore, we need to search for another origin and explore routes for the catalyst's inhibition.

The inhibition reaction path (**II**) to (**III-b**) in Scheme 1 involving ethylene, was studied for the three monochlorinated anions (Figure 2, left). The activation energies show that this path is kinetically disfavored with respect to the oligomerization: the difference between the two barriers ($\Delta G^{\ddagger}_{b} - \Delta G^{\ddagger}_{a}$) is +6.9, +9.0 and +23.4 kcal·mol^{-1}. Moreover, all reactions are endergonic: 9.1, 18.0 and 21.6 kcal·mol^{-1} for TMA, $[PhOAlMe_2]_2$ and $[AlMeO]_6[AlMe_3]$ respectively. Note that energies are relative to the energy of the ion-pair and the ethylene molecule at infinite distance. Hence, this inhibition reaction is unlikely to happen in the presence of ethylene.

We then investigated an alternative inhibition path that could take place before the ethylene uptake, e.g., the iron methylation: reaction (**I**) to (**III-c**) in Scheme 1. However, the calculations reveal that product (**III-c**) is unstable for all three monochlorinated anions and spontaneously dissociates to (**I**).

A third inhibition path, (**I**) → (**III-d**) in Scheme 1 has been considered. The chlorinated dimeric TMA anion is already partially dissociated in the presence of the cationic iron species. The complete dissociation of TMA (Eq. 1) requires ΔG_{diss} = +4.5 kcal·mol^{-1} for the monochlorinated TMA dimer (R=Me) and even is exothermic for the dichlorinated anion (R=Cl): ΔG_{diss} = –7.5 kcal.mol^{-1}.

$$[LFeMe]^{+} \cdots [AlMe_3][AlMe_2RCl]^{-} \rightarrow AlMe_3 + [LFeMe]^{+} \cdots AlMe_2RCl]^{-} \quad (1)$$

The subsequently generated $AlMe_3$ easily coordinates to the $[LFe(II)Me]^{+}$ in presence of the anionic $[AlMe_2RCl]^{-}$ species by forming two bridging methyl groups between the Al and iron center (the methyl group of $[LFe(II)Me]^{+}$ and one of the AlM_3 methyl groups, Figure 7S) forming

III-d, thereby consuming the vacant site that is required for ethylene coordination. The overall reaction is exergonic by –4.7 in the presence $[AlMe_3Cl]^-$ and –8.6 kcal.mol^{-1} in the presence of $[AlMe_2Cl_2]^-$. This coordination of $AlMe_3$ could therefore be responsible for the poisoning of the catalyst. Moreover, ethylene is not sufficiently nucleophilic to replace the TMA monomer, as was concluded from a relaxed coordinate scan[2], where the interchange of TMA with ethylene costs more than 18 kcal·mol^{-1}. These results seem to contradict the work of Bryliakov *et al* [25]. Nonetheless, they studied the iron 2,6-bis(2,6-diisopropylphenylimino)ethyl-pyridine catalyst, which experimentally can be activated by TMA, whereas we focused on the 2,6-bis(2-methylphenylimino) analogue, which is experimentally inactive with TMA. Accordingly, our calculations explain these experimental findings by the fact support that the TMA association (eq. 2) is exergonic (–4.7 kcal·mol^{-1}) for the bis(methylphenyl) complex, while it is endergonic (+5.6 kcal·mol^{-1}) for the bis(diisopropyl) complex, likely due to the steric hindrance of the bulky isopropyl groups.

$$[Al_2Me_6Cl)]^-\cdots[LFeMe]^+ \rightarrow [AlMe_3Cl)]^-\cdots[LFeMe.AlMe_3]^+ \qquad (2)$$

The dissociation reaction (eq. 1) with $[PhOAlMe_2][PhOAlClRMe_2]$ is unlikely to occur since the complete dissociation costs +15.3 kcal·mol^{-1} for the monochlorinated (R=Me) and +19.9 kcal·mol^{-1} for the dichlorinated anion (R=Cl). Moreover, in the former case a relaxed coordinate analysis, where the Al-Al distance is stepwise increased, shows a barrier of about 25 kcal·mol^{-1}

[2] In this relaxed coordinate scan the *r*(Fe-Al) distance is constrained but systematically increased in steps of 0.5 Å, while all other atoms are relaxed (Figure 3S). Even at *r*(Fe-Al) = 10 Å the scan shows a tendency of increasing energy, taking the fully relaxed structure as a reference. We were not able to locate the transition state on the potential energy surface.

to generate the mononuclear Lewis acid Me_2AlOPh that could deactivate the catalyst.[3] Since this inhibition reaction is in direct competition with the ethylene insertion (24.9 kcal·mol^{-1} energy barrier, but exergonic (ΔG_r^{ins} = –10.9 kcal·mol^{-1}) the insertion reaction clearly is favored. We can therefore reasonably assume that this inhibition route is unlikely to take place. In the case of the MAO all aluminum atoms are tetravalent, thus lacking the possibility to coordinate to methyl on the iron center, making this inhibition reaction improbable.

4. Conclusions

In summary, we have identified $[PhOAlMe_2]_2$ as cocatalyst able to activate iron bis(imino)pyridine precatalysts. This well-defined cocatalyst allowed us to unravel the ethylene insertion and inhibition mechanisms of the active species by DFT calculations. These key mechanisms were further extended to a representative MAO model and TMA and furnish a quantified analysis of the experimental ranking of the three cocatalysts: MAO > $[PhOAlMe_2]_2$ >> TMA.

We conclude that efficient cocatalysts should be able to generate a cationic alkylated iron species, whereby the cocatalyst itself is turned into a chlorinated anion. It seems that this anion then should weakly interact, since lower barriers are observed for anions with smaller cationic π-complex/anion dissociation energies and having higher activities. Additionally, the cocatalyst should not contain (or easily generate) trivalent reactive aluminum sites (such as in TMA) that could form adducts with the already generated cationic methylated iron species, thereby

[3] We were unable to locate the transition state on the potential energy surface.

poisoning the catalyst. We hope that these results help for a more rational understanding of the role of cocatalysts in oligomerization reactions and may open new routes for the molecular design of improved cocatalysts.

Supporting Information.

Computational details, cocatalyst synthesis, catalytic experiments, geometrical features of intermediates and transition states, and Cartesian coordinates of all fully-optimized geometries.

References

[1] A. Andresen, H.-G. Cordes, J. Herwig, W. Kaminsky, A. Merck, R. Mottweiler, J. Pein, H. Sinn, H.-J. Vollmer, Angew. Chemie Int. Ed. English 15 (1976) 630.

[2] W. Kaminsky, H.-J. Vollmer, R. Woldt, Process for Producing Polymers and Copolymers of Ethylene, DE3007725A1, 1980.

[3] H. Sinn, W. Kaminsky, H.-J. Vollmer, R. Woldt, Angew. Chemie Int. Ed. 19 (1980) 390.

[4] W. Kaminsky, Macromolecules 45 (2012) 3289.

[5] A. Boudier, P.-A.R. Breuil, L. Magna, H. Olivier-Bourbigou, P. Braunstein, Chem. Commun. (Camb). 50 (2014) 1398.

[6] B.L. Small, M. Brookhart, J. Am. Chem. Soc. 120 (1998) 7143.

[7] G.J.P. Britovsek, V.C. Gibson, B.S. Kimberley, P.J. Maddox, S.J. McTavish, G.A. Solan, A.J.P. White, D.J. Williams, Chem. Commun. (1998) 849.

[8] V.C. Gibson, C. Redshaw, G.A. Solan, Chem. Rev. 107 (2007) 1745.

[9] C. Bianchini, G. Giambastiani, L. Luconi, A. Meli, Coord. Chem. Rev. 254 (2010) 431.

[10] L. Xiao, R. Gao, M. Zhang, Y. Li, X. Cao, W.-H. Sun, Organometallics 28 (2009) 2225.

[11] B.L. Small, R. Rios, E.R. Fernandez, D.L. Gerlach, J.A. Halfen, M.J. Carney, Organometallics 29 (2010) 6723.

[12] A. Boudier, P.A.R. Breuil, L. Magna, C. Rangheard, J. Ponthus, H. Olivier-Bourbigou, P. Braunstein, Organometallics 30 (2011) 2640.

[13] M.J. Hanton, K. Tenza, Organometallics 27 (2008) 5712.

[14] P. Hao, Y. Chen, T. Xiao, W.-H. Sun, J. Organomet. Chem. 695 (2010) 90.

[15] M. Zhang, P. Hao, W. Zuo, S. Jie, W.-H. Sun, J. Organomet. Chem. 693 (2008) 483.

[16] M.R. Mason, J.M. Smith, S.G. Bott, A.R. Barron, J. Am. Chem. Soc. 115 (2002) 4971.

[17] T.K. Trefz, M.A. Henderson, M.Y. Wang, S. Collins, J.S. McIndoe, Organometallics 32 (2013) 3149.

[18] E. Zurek, T. Ziegler, Inorg. Chem. 40 (2001) 3279.

[19] E. Zurek, T. Ziegler, Faraday Discuss. 124 (2003) 93.

[20] E. Zurek, T. Ziegler, Prog. Polym. Sci. 29 (2004) 107.

[21] G.J.P. Britovsek, V.C. Gibson, S.K. Spitzmesser, K.P. Tellmann, A.J.P. White, D.J. Williams, J. Chem. Soc. Trans. (2002) 1159.

[22] K.P. Bryliakov, N. V Semikolenova, V.A. Zakharov, E.P. Talsi, Organometallics 23 (2004) 5375.

[23] M.W. Bouwkamp, E. Lobkovsky, P.J. Chirik, J. Am. Chem. Soc. 127 (2005) 9660.

[24] R. Raucoules, T. de Bruin, P. Raybaud, C. Adamo, Organometallics 27 (2008) 3368.

[25] K.P. Bryliakov, E.P. Talsi, N. V Semikolenova, V.A. Zakharov, Organometallics 28 (2009) 3225.

[26] K.P. Bryliakov, E.P. Talsi, Coord. Chem. Rev. 256 (2012) 2994.

[27] D. Ogrin, S.G. Bott, A.R. Barron, J. Chem. Crystallogr. 38 (2008) 397.

[28] C. Gorl, H.G. Alt, J. Organomet. Chem. 692 (2007) 4580.

[29] Y. Zhao, D.G. Truhlar, Theor. Chem. Acc. 120 (2007) 215.

[30] Z. Boudene, T. De Bruin, H. Toulhoat, P. Raybaud, Organometallics 31 (2012) 8312.

[31] P.J. Hay, W.R. Wadt, J. Chem. Phys. 82 (1985) 270.